

Journal of Materials Chemistry A

Materials for energy and sustainability

Accepted Manuscript

This article can be cited before page numbers have been issued, to do this please use: A. Henrique, P. Dutta, M. Gupta, G. Mouchaham, Y. Magnin, C. Serre, G. Maurin and J. A. C. Silva, *J. Mater. Chem. A*, 2026, DOI: 10.1039/D6TA01917J.



This is an Accepted Manuscript, which has been through the Royal Society of Chemistry peer review process and has been accepted for publication.

Accepted Manuscripts are published online shortly after acceptance, before technical editing, formatting and proof reading. Using this free service, authors can make their results available to the community, in citable form, before we publish the edited article. We will replace this Accepted Manuscript with the edited and formatted Advance Article as soon as it is available.

You can find more information about Accepted Manuscripts in the [Information for Authors](#).

Please note that technical editing may introduce minor changes to the text and/or graphics, which may alter content. The journal's standard [Terms & Conditions](#) and the [Ethical guidelines](#) still apply. In no event shall the Royal Society of Chemistry be held responsible for any errors or omissions in this Accepted Manuscript or any consequences arising from the use of any information it contains.

MFU-4 as a Benchmark Molecular Sieve for Efficient CO_2/CH_4 Separation in Biogas Upgrading

Adriano Henrique^a, Prantar Dutta^{b,c}, Mayank Gupta^d, Georges Mouchaham^{d*},
Yann Magnin^c, Christian Serre^d, Guillaume Maurin^{b,e*} and José A. C. Silva^{a*}

^a Centro de Investigação de Montanha (CIMO), Instituto Politécnico de Bragança, Campus Santa Apolónia, 5300-253 Bragança, Portugal

^b ICGM, Univ. Montpellier, CNRS, ENSCM, Montpellier, France

^c OneTech, R&D, CSTJF, TotalEnergies, Pau 64018, France

^d Institut des Matériaux Poreux de Paris, ESPCI Paris, Ecole Normale Supérieure, CNRS, PSL University, Paris 75005, France

^e Institut Universitaire de France, France

* Corresponding Authors: Georges Mouchaham (georges.mouchaham@ens.psl.eu),
Guillaume Maurin (guillaume.maurin1@umontpellier.fr), José A. C. Silva
(jsilva@ipb.pt)



Abstract

View Article Online
DOI: 10.1039/D6TA01917J

The efficient separation of CO₂ from CH₄ is central to industrial biogas upgrading for the production of pipeline-quality biomethane. Kinetic, molecular sieve-based adsorption is preferred over thermodynamic approaches, making small-pore adsorbents such as CMS-3K and ion-exchanged ETS-4 the current industrial standard. Here, we show, through a combination of breakthrough experiments and computational analysis, that the ultra-microporous Zn triazolate MOF MFU-4 significantly surpasses these benchmarks. Its unique architecture, featuring alternating small and large cages connected by narrow, square-shaped pore gates, kinetically hinders CH₄ diffusion while facilitating rapid CO₂ transport and achieving high CO₂ uptake, effectively overcoming the long-standing trade-off between CO₂/CH₄ selectivity and CO₂ capacity. As a result, MFU-4 achieves CO₂/CH₄ kinetic selectivity up to twice that of ETS-4 and four times that of CMS-3K, with CO₂ working capacities up to seven and four times higher, respectively, over the 100–500 kPa range, and an exceptional CO₂ uptake of ~7.4 mol·kg⁻¹ at 298 K and 500 kPa. These findings establish MFU-4 as an excellent molecular sieve for biogas upgrading, delivering performance far beyond current industrial standards.



1 Introduction

View Article Online
DOI: 10.1039/D6TA01917J

The upgrading of biogas, primarily a mixture of methane (CH_4) and carbon dioxide (CO_2), into pipeline-quality biomethane, a high-value natural-gas substitute, has emerged as a critical process for both renewable energy production and greenhouse-gas mitigation.^[1,2] Efficient removal of CO_2 from the CH_4 -rich stream not only enhances the calorific value of the purified gas but also decreases volumetric flow, thereby, reducing transportation and compression costs while facilitating downstream processing and handling.^[3,4] With the growing pressure on circular economy principles and low-carbon energy solutions, adsorption-based technologies for CO_2/CH_4 separation have garnered substantial attention as energy-efficient alternatives to conventional energy-intensive approaches such as water scrubbing, amine absorption and cryogenic processes.^[4-6]

In this context, several adsorbent materials have been explored for CO_2/CH_4 separation, predominantly leveraging thermodynamic (equilibrium-driven) selectivity, where CO_2 is preferentially adsorbed due to its high polarizability and quadrupole moment which promote stronger interactions with the host frameworks compared to CH_4 . Among these, zeolites such as 13X,^[7-14] 4A,^[11,15-18] 5A,^[19-22] together with a wide variety of ion-exchanged derivatives,^[23-32] have long been regarded as benchmark adsorbents. Their prominence arises from well-defined microporous frameworks and strong CO_2 affinity, which arises from specific interactions between CO_2 molecules and extra-framework cations, as well as from confinement effects within their uniform pore structures. More recently, metal-organic frameworks (MOFs)^[33] have emerged as highly tunable alternative porous adsorbents, offering the unprecedented ability to precisely tailor pore size, shape and chemical functionality to enhance interactions with CO_2 . Representative examples include extended MOF-74 and its amine-grafted frameworks,^[34-40] which exhibit high CO_2 uptake due to strong interactions with open metal sites and/or amine functionalities, as well as small-pore MOFs such as MIL-120(Al),^[41-43] CALF-20(Zn),^[44] and NbOFFIVE-1-Ni,^[45] where CO_2 affinity is largely governed by molecular confinement within the pores.

Despite its advantages, this equilibrium-based adsorption strategy often entails substantial energy penalties during adsorbent regeneration and may lead to diminished CH_4 recovery, particularly under cyclic operation. In such cases, processes such as Vacuum Pressure Swing Adsorption (VPSA) are typically required to fully regenerate and reset the adsorption bed, further increasing operational complexity and energy demand. These limitations highlight the need for the development of next-generation adsorbents and separation strategies that



simultaneously deliver high selectivity, low regeneration energy requirements, and robust operational stability, thereby enabling more sustainable and economically viable biogas upgrading processes. Accordingly, kinetic separation mechanisms offer an attractive alternative to purely equilibrium-driven strategies. In this approach, selectivity originates from differences in diffusion rates or mass-transfer kinetics, driven by variations in adsorption strength and/or steric constraints imposed by the pore dimensions relative to molecular size. Faster-diffusing species are preferentially transported, enabling operation at high feed velocities and short cycle times. Importantly, because CH₄ is only weakly adsorbed, regeneration requirements are significantly reduced, lowering purge demand and overall energy consumption.^[46,47] As a result, CH₄ can be efficiently recovered in the raffinate stream with minimal losses to the adsorbent phase.

In this context, two materials have emerged as industrial benchmarks, illustrating the practical viability of diffusion-controlled separations for scalable biogas upgrading. The first is the carbon molecular sieve CMS-3K (commercially supplied by Takeda/Osaka Gas), which displays rapid CO₂ adsorption, whereas CH₄ uptake can require several days to reach equilibrium, reflecting pronounced kinetic hindrance for CH₄ diffusion.^[48,49] This behavior originates from the ultra-small pore entrances of CMS-3K, whose dimensions closely approach the kinetic diameter of CH₄, thereby imposing a strong mass-transfer resistance at the micropore apertures. CMS materials are currently deployed in industrial VPSA processes, including the METHAGEN systems commercialized by SysAdvance.^[50,51] The second benchmark material, the zeotype ETS-4 (Engelhard Titanosilicate-4), modified with alkaline-earth cations, similarly exploits precise pore-aperture tuning to introduce diffusion barriers or molecular sieving effects that restrict CH₄ while favouring smaller or more rapidly diffusing species such as N₂ or CO₂.^[52–56] ETS-4 is widely implemented under the Molecular Gate® technology, a registered trademark of BASF Catalysts LLC and exclusively licensed to Guild Associates.^[57] Despite their clear industrial relevance, both materials exhibit relatively modest equilibrium CO₂ adsorption capacities (< 3 mol·kg⁻¹ at 500 kPa).^[48,49,56] Consequently, deep vacuum levels (10–20 kPa) are required during regeneration to achieve practical working capacities.^[58] This dependence on vacuum-intensive operation increases energy demand and process complexity, elevating both capital and operating expenditures (CAPEX and OPEX) and ultimately limiting overall process efficiency.

To overcome these limitations and move beyond the intrinsic trade-off between CO₂/CH₄ kinetic selectivity and CO₂ uptake, alternative classes of materials must be explored. In this



regard, ultra-small pore MOFs offer a unique platform to transcend this long-standing compromise, enabling the rational design of diffusion barriers or dynamic pore-gating mechanisms that selectively regulate molecular transport, enabling rapid CO₂ diffusion while kinetically restricting CH₄, all without sacrificing adsorption capacity within larger internal cavities. Guided by this design principle, we conducted a systematic examination of MOF structural databases and identified MFU-4(Zn)^[59] (Metal–Organic Framework Ulm University-4) as a particularly promising candidate. Its framework, constructed from Zn-based secondary building units interconnected by benzo[1,2-d:4,5-d']bistriazolate ligands, features an alternating arrangement of small (~4 Å) and large (~12 Å) cages interconnected through ultranarrow, square-shaped pore apertures delimited by four chloride atoms with a limiting diameter of approximately 2.5 Å (Figure 1a and Figure 1b). This precise integration of confined apertures and spacious cavities creates an architecture ideally suited to impose strong kinetic constraints on CH₄ diffusion while maintaining fast CO₂ transport and high CO₂ uptake within the larger cages.

To validate this concept, we employed a synergistic combination of advanced breakthrough experiments and computational methods, demonstrating that MFU-4(Zn) surpasses the industrial benchmark adsorbents CMS-3K and ETS-4 in CO₂/CH₄ separation

2 Methodology

2.1 Synthesis and Characterization

Synthesis

The H₂-BBTA linker was synthesized according to previously reported procedures, starting from 1,5-dichloro-2,4-dinitrobenzene.^[59,60] MFU-4 was synthesized in solvothermal conditions by dissolving anhydrous ZnCl₂ (136 mg, 1.00 mmol) and H₂-BBTA (40 mg, 0.25 mmol) in 4 mL of DMF, transferring the solution to a screw-capped glass pressure tube, and heating at 140 °C for 3 days, followed by cooling to room temperature. The supernatant was removed, and the yellow microcrystalline solid was washed with DMF (3 × 1 mL) and dried in air to afford 65 mg (≈0.056 mmol, 28%) of MFU-4. The product consisted mainly of cubic microcrystals, with a smaller fraction of octahedral crystals, as observed by SEM (see discussion below).

Characterization



The FT-IR spectrum of the non-activated pristine MFU-4 confirms the successful formation of the Zn–bistriazolate framework and provides clear evidence for the presence of residual guest molecules within the pores (Figure S1). In particular, a strong absorption band at $\sim 1652\text{ cm}^{-1}$ is assigned to the C=O stretching vibration of DMF, indicating that DMF molecules remain confined within the framework after synthesis. Additional bands at ~ 2918 and $\sim 2848\text{ cm}^{-1}$ corresponding to aliphatic C–H stretching further support the presence of occluded solvent molecules (see Section S1.1.1).

The phase purity of the synthesized MFU-4 was confirmed by powder X-ray diffraction (PXRD). The PXRD pattern of the as-synthesized MFU-4 matches well with the simulated pattern generated from the reported single-crystal structure, with all characteristic reflections appearing at the same 2θ positions (Figure S2). PXRD patterns recorded for materials after activation and CO₂ adsorption remain the same as the pristine material indicating that MFU-4 maintains its structural integrity and exhibits excellent stability (Figure S3).

The scanning electron microscopy (SEM) images of the as-synthesized MFU-4 (Figure S4) reveal the presence of well-faceted microcrystalline particles exhibiting two distinct morphologies, namely predominantly blocky/cubic-shaped crystals together with a smaller fraction of octahedral crystallites. These morphologies are identified based on their characteristic geometrical features and faceted structures observed in SEM, which reflect different crystal growth habits under solvothermal conditions. The particle size lies in the micrometer range ($\sim 0.5\text{--}5\text{ }\mu\text{m}$), with most crystals typically between $1\text{--}3\text{ }\mu\text{m}$. While an accurate quantitative phase fraction cannot be extracted from SEM images, the cubic morphology is clearly dominant, with octahedral crystals present in lower proportion. To further confirm that both morphologies correspond to the same phase, energy-dispersive X-ray (EDX) analysis was performed on individual crystals. The measured Zn and Cl atomic percentages (Zn $\approx 52.53\text{ at\%}$, Cl $\approx 47.47\text{ at\%}$) correspond to Zn:Cl ratios of $\sim 1:0.85$ and ~ 1.09 for cubic and octahedral crystals, respectively, which are in good agreement with the expected MFU-4 stoichiometry. This confirms that both morphologies belong to the same framework rather than different phases or impurities.

Thermogravimetric analysis (TGA) was performed to evaluate the purity, thermal behavior, and guest (DMF) content of MFU-4 in its as-synthesized form. The TGA profile exhibits a characteristic multistep weight-loss behavior consistent with previous reports and aligns well with the formulation $[\text{Zn}_5\text{Cl}_4(\text{BBTA})_3]\cdot 3\text{DMF}\cdot 6\text{H}_2\text{O}$ (Figure S5). Three distinct weight-loss steps are observed. An initial weight loss of $\sim 9\text{ wt\%}$ below $\sim 80\text{ }^\circ\text{C}$ is attributed to the removal of surface-adsorbed moisture and residual lattice water. A second weight loss of ~ 18



wt% in the temperature range of 120–300 °C corresponds to the release of approximately three DMF molecules per formula unit, in good agreement with the theoretical DMF content (~17.18 wt%), confirming that the as-synthesized material is obtained in a solvated state. At higher temperatures (above ~420 °C), a major weight loss (~49 wt%) is observed due to framework decomposition. After activation at 250 °C, the TGA curves recorded for MFU-4 following CO₂ and N₂ sorption measurements (Figure S6) differ significantly from those of the as-synthesized sample. In particular, the characteristic weight loss associated with DMF in the 120–300 °C range disappears, confirming the complete removal of pore-confined solvent molecules and the formation of the desolvated framework. However, a low-temperature weight loss remains and is significantly increased. This behavior arises from the re-adsorption of moisture upon exposure of the activated sample to ambient air. Once DMF is removed, the internal pore volume becomes fully accessible, enhancing the affinity of the framework toward water. Quantitatively, the low-temperature weight loss increases from ~9 wt% in the as-synthesized sample to approximately 25–27 wt% in the activated sample, clearly indicating substantial water uptake after activation. This increase reflects the replacement of DMF by adsorbed water molecules within the accessible pores. Importantly, the absence of the intermediate weight-loss step confirms that no DMF remains after activation, and the observed low-temperature loss is solely due to physically adsorbed moisture. This behavior is consistent with literature reports on activated MOFs, where exposure to air leads to rapid water uptake and increased low-temperature mass loss (see Section S1.1.4).

2.2 Fixed Bed Breakthrough Experiments

The single-component adsorption equilibrium data of CO₂ was measured using a chromatographic technique based on dynamic fixed-bed breakthrough experiments. The experimental setup comprises three main sections: (1) gas preparation, (2) adsorption, and (3) analysis. In the gas preparation section, He carrier gas and CO₂ were fed through mass flow controllers, while system pressure was set by back-pressure regulators. The adsorption section contained a stainless-steel column filled with the agglomerated MFU-4 and placed inside a temperature-controlled water bath. The outlet from the fixed bed was directed to the analytical section, where a gas chromatograph equipped with a thermal conductivity detector (TCD) which continuously monitored the CO₂ concentration. For CO₂/CH₄ binary breakthrough experiments, the same procedure was applied. In this case, the feed gas mixture was set in the gas preparation section, and a pre-programmed six-port valve periodically directed aliquots of the outlet stream



to a packed column for peak separation before analysis by the TCD detector. Further details on the setup, procedure, and operating conditions are provided in the Supporting Information. View Article Online
DOI: 10.1039/D6TA01917J

2.3 Modelling and Numerical Simulations

The Aspen Adsorption v11 package^[61] was employed to numerically simulate the binary breakthrough experiments. Input data for these simulations were obtained from adsorption equilibrium data (experimental for CO₂ and simulated for CH₄), modelled using the Dual-Site Langmuir (DSL) isotherm.^[62] To analyze mass transfer kinetics, a linear driving force (LDF) model was applied,^[63] which is based on the solid-phase concentration gradient and has been satisfactorily validated in previous studies.^[64,65] Complete details of the assumptions, model equations, parameter correlations, and numerical procedures used to solve the partial differential equations (PDEs) are provided in the Supporting Information.

2.4 Molecular Simulations and Quantum Calculations

The crystal structure of MFU-4 was geometry-optimized using periodic density functional theory (DFT) as implemented in the Vienna Ab initio Simulation Package (VASP).^[66] Calculations were performed using the Perdew-Burke-Ernzerhof (PBE) exchange-correlation functional^[67] in conjunction with projector-augmented wave (PAW) pseudopotentials^[68] and Grimme's D3 dispersion correction with Becke-Johnson damping.^[69,70] Both atomic positions and lattice parameters were relaxed using the conjugate-gradient algorithm with a plane-wave energy cutoff of 600 eV. Convergence criteria of 10⁻⁶ eV for the total energy and 0.01 eV/Å for atomic forces were applied. Brillouin-zone sampling was carried out using a 2×2×2 Monkhorst-Pack k-point mesh.^[71] The electronic charge density of the optimized structure was subsequently used to derive atom-centered partial charges using the DDEC6 method, as implemented in the ChgemoL package.^[72-75]

Grand canonical Monte Carlo (GCMC) simulations were first performed to predict the single component adsorption isotherms of CO₂ and CH₄ in MFU-4 at three temperatures (298 K, 313 K, and 343 K) and pressures up to 500 kPa. CO₂ and CH₄ were modeled using the EPM2^[76] and TraPPE united-atom^[77] force fields, respectively, while Lennard-Jones (LJ) parameters for the framework atoms were taken from the Universal Force Field (UFF).^[78] LJ interactions between the adsorbates and the octahedrally coordinated Zn atoms were excluded, as these metal centers are deeply shielded within the Kuratowski-type nodes and are effectively inaccessible to guest molecules. Lorentz-Berthelot mixing rules were applied for cross-interactions. Simulations were performed in a 2×2×2 supercell, employing a cutoff distance of 12 Å for both van der Waals and electrostatic host-guest interactions. Long-range electrostatic interactions were treated using



the Ewald summation method. For each pressure point, 2×10^7 Monte Carlo cycles were used for both equilibration and production. All GCMC simulations were performed using Complex Adsorption and Diffusion Simulation Suite (CADSS).^[79] The adsorption enthalpies at zero coverage for CO₂ and CH₄ were also calculated using the revised Widom's test particle insertion method.^[80] The LJ parameters and partial charges for the atoms of MFU-4 and both adsorbates are provided in Tables S2 and S3, respectively.

The energy barrier associated with crossing the pore gate of MFU-4, which separates alternating large and small cages, was evaluated for both CO₂ and CH₄ using climbing-image nudged elastic band (CINEB)^[81] calculations as implemented in the Quickstep module of the CP2K package.^[82] The calculations employed the PBE functional with D3/Becke-Johnson dispersion correction, together with triple- ζ valence polarized (TZVP) Gaussian basis sets^[83] and Goedecker–Teter–Hutter (GTH) pseudopotentials^[84,85] for all atoms. An auxiliary plane-wave cutoff of 500 Ry was used. To model migration across the pore gate, a supercell containing two unit cells along the *a*-direction was constructed. The initial and final states were generated by placing a single adsorbate molecule (CO₂ or CH₄) on either side of the pore gate, followed by full relaxation of atomic positions. The minimum-energy pathway was resolved using seven intermediate images, with a force convergence criterion of 5×10^{-4} Hartree.

3 Results and Discussion

The equilibrium single component CO₂ adsorption isotherms of MFU-4 were derived from breakthrough experiments performed at 298 K, 313 K, and 343 K over pressures up to 500 kPa (see Table S4 and Figure S8). The experimentally obtained equilibrium data are compared with the corresponding GCMC simulated adsorption isotherms in Figure 1c. At all three temperatures, experimental and simulated isotherms are in good agreement and exhibit a characteristic IUPAC Type I profile typical of microporous adsorbents, with a steep increase in CO₂ uptake at low partial pressures followed by a gradual approach to saturation.^[86] The moderately rounded “knee” of the isotherm suggests the presence of more than one adsorption environment. The DSL model provides a robust description of the experimental data over the entire pressure range, indicating that CO₂ adsorption can be rationalized by two families of adsorption sites with comparable affinities but different saturation capacities (see Table S6 for the fitted parameters). This interpretation is supported by the analysis of GCMC configurations which reveals two distinct adsorption sites, one near the Cl atoms delimiting the pore gates and a second situated within the larger cages (Figure 1d) (see Figure S10 for more details). The isosteric heat of adsorption (Q_{st}) for CO₂, estimated using the Clausius–Clapeyron relation



(Figure S12), remains essentially constant over the investigated loading range, at $\sim 24.7 \text{ kJ}\cdot\text{mol}^{-1}$ in line with the previously reported experimental values ($\sim 24.4 \text{ kJ}\cdot\text{mol}^{-1}$)^[87] and our simulated adsorption enthalpy at infinite dilution ($\sim 24 \text{ kJ}\cdot\text{mol}^{-1}$).

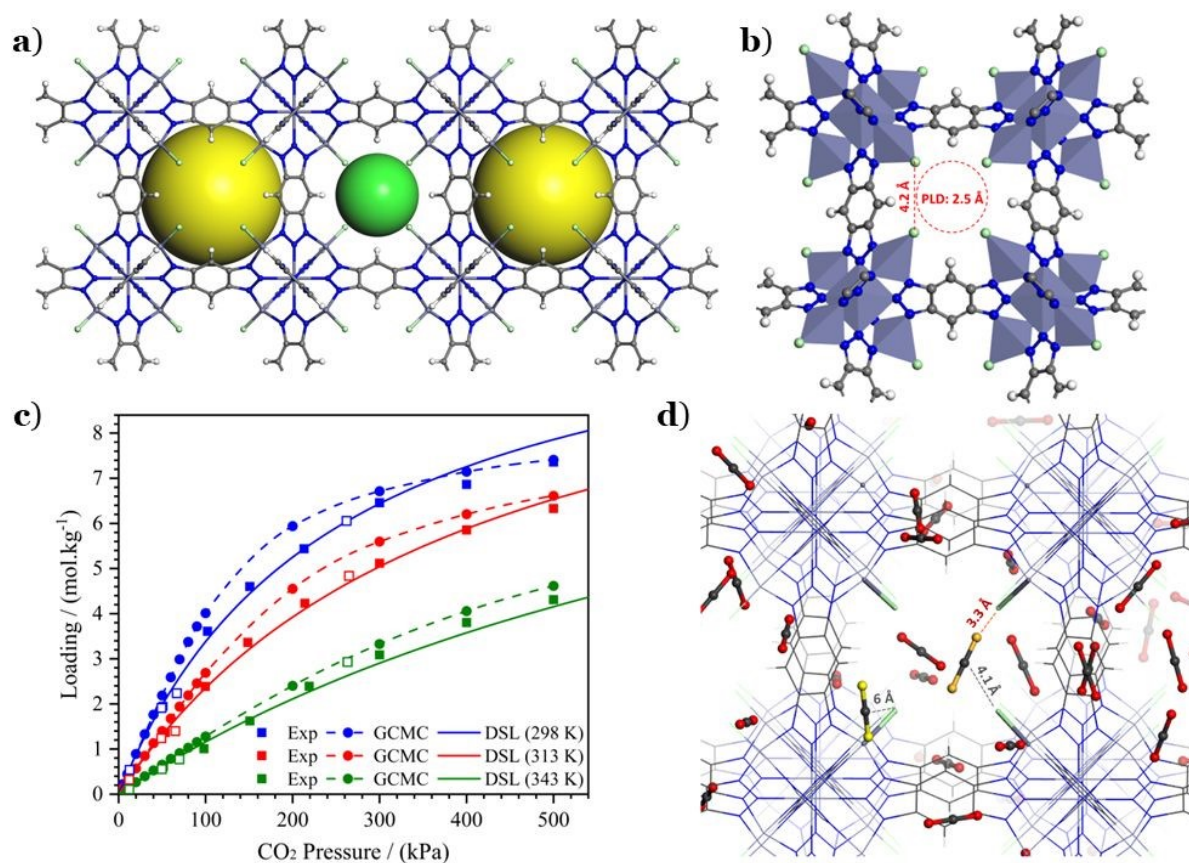


Figure 1. (a) Pore network of MFU-4 with alternating large (yellow spheres) and small (green sphere) cages. (b) Square-shaped pore gate, with pore limiting diameter of 2.5 Å, separating the cages. (c) Equilibrium single-component CO₂ adsorption isotherms on MFU-4 in the temperature range of 298-343 K. Filled symbols: single-component experimental data; open symbols: CO₂ loadings obtained from binary breakthrough experiments; symbols and dashed: GCMC simulations; continuous lines: DSL thermodynamic model fit. (d) Microscopic mechanism of CO₂ adsorption in MFU-4 illustrated by a representative GCMC snapshot from simulations at 100 kPa. Two CO₂ molecules with the shortest MOF-CO₂ distances for each adsorption site are highlighted — one adsorbed at the pore gate (O_{CO₂} in orange; Cl-C_{CO₂} distance: 4.1 Å) and one located inside the large cage (O_{CO₂} in yellow; Cl-C_{CO₂} distance: 6 Å).

Adsorption of CH₄ in MFU-4 could not be detected using the flow chromatographic method, most likely due to its extremely slow diffusion within the MOF, resulting in breakthrough times that occur almost simultaneously with the gas residence time in the fixed bed. To validate this hypothesis, DFT-CINEB calculations were performed to quantify the



energy barriers for guest migration across the pore gates of MFU-4. Minimum energy pathways (MEPs) were determined by positioning a guest molecule on either side of an individual pore gate as the initial and final states. The resulting MEPs for CH₄ and CO₂ crossing the pore gate are shown in Figures 2a and 2b, respectively. CH₄ faces a substantial energy barrier of ~53 kJ·mol⁻¹, with a well-defined transition state at the centre of the gate. This large barrier reflects severe steric hindrance, as the spherical CH₄ molecule (kinetic diameter ~3.8 Å) must pass through a square aperture with a pore limiting diameter of only ~2.5 Å. In contrast, the MEP for CO₂ shows the pore gate as a local energy minimum rather than a transition state. The square gate provides confinement-enhanced stabilization for the linear CO₂ molecule, consistent with GCMC simulations that identify the gate region as the primary adsorption site. Transport of CO₂ between adjacent cages is therefore not limited by an enthalpic barrier but is instead controlled by entropic constraints arising from confinement and molecular orientation. These findings suggest that MFU-4 can achieve size selective CO₂ adsorption over CH₄ via a predominantly kinetically controlled mechanism.

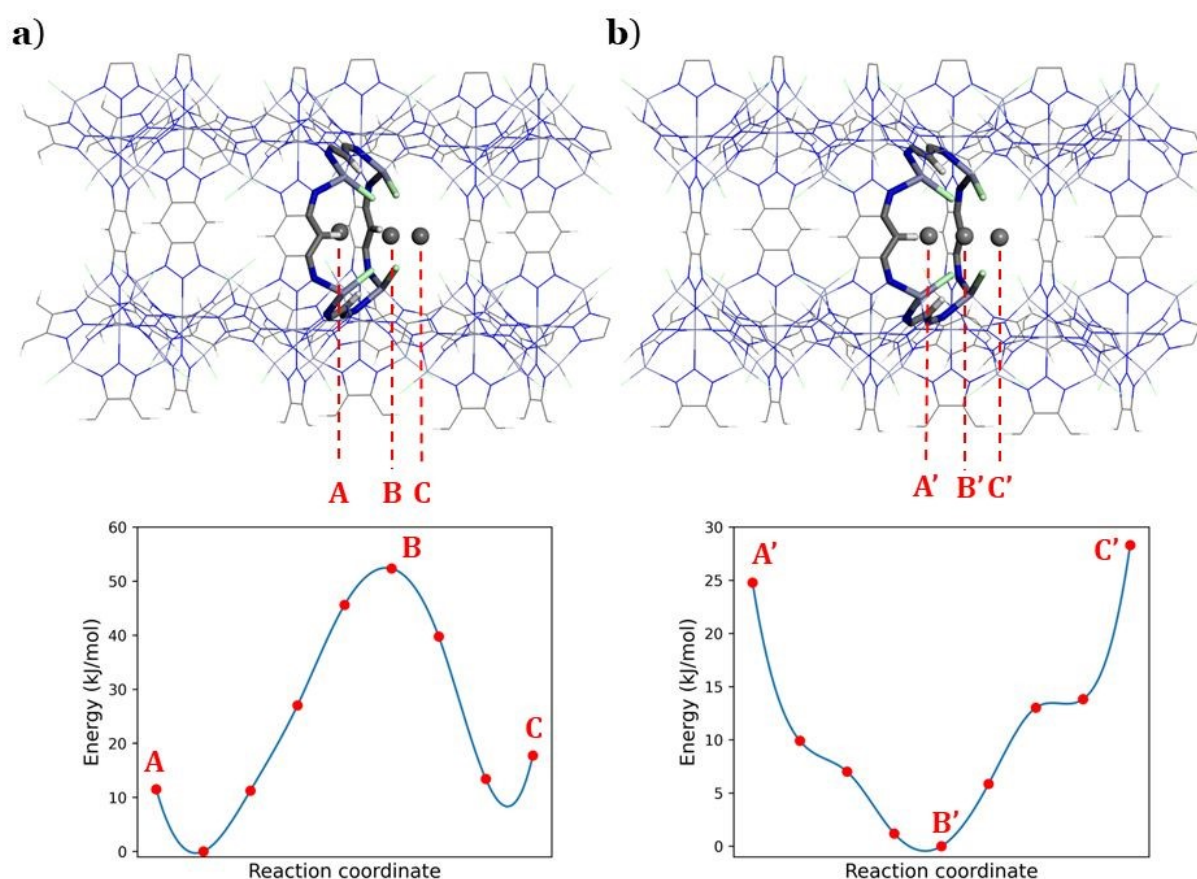
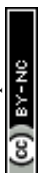


Figure 2. Minimum-energy pathways for (a) CH₄ and (b) CO₂ migration across the pore gate (highlighted by thicker sticks) from the large cage to the small cage of MFU-4, obtained from DFT-based CINEB calculations. The molecules are represented only by their respective center



of mass (carbon atom) for convenience of visualization. For CH₄, points A, B, and C represent the initial state, transition state, and final state, respectively. For CO₂, points A', B', and C' correspond to the initial state, a local energy minimum at the pore gate, and the final state. In both cases, A (A') lies within the large cage, B (B') at the center of the pore gate, and C (C') at the center of the smaller cage.

As a further step, we experimentally investigated the competitive adsorption of CO₂ and CH₄ under dynamic flow conditions. Accordingly, breakthrough experiments were performed for CO₂/CH₄ mixtures of 50:50 and 10:90 at total pressures of 100 and 500 kPa in the same range of temperature covered in the single-component adsorption measurements (see Table S7 for experimental conditions) under typical biogas upgrading conditions for PSA cyclic adsorption. These feed compositions provide a simple and industry-relevant reference condition, where the selected pressure interval reflects practical CO₂ capture and upgrading conditions of the feed to produce pure CH₄, near room temperature and at atmospheric to moderately elevated pressures relevant for cyclic PSA operation. It should be noted that, although raw biogas streams may contain trace contaminants such as H₂S and water, these species are typically removed during upstream conditioning, including desulfurization and dehydration steps (e.g., guard beds). This is standard practice in commercial biogas upgrading systems, ensuring that the feed entering the adsorption unit is effectively dry and free of contaminants that could compromise the performance of the core process. In contrast to post-combustion streams, which are often treated directly under humid conditions, biogas streams are routinely pre-conditioned prior to separation.

Representative breakthrough curves for CO₂/CH₄ mixtures at 298 K are shown in Figure 3. In all cases, CH₄ elutes almost immediately at the residence time of the gas in the column, indicating that the bulk CH₄ stream bypasses the adsorbent due to strong diffusional limitations as revealed by the DFT-derived MEPs. By contrast, CO₂ exhibits a clear and well-defined adsorption front, with the expected breakthrough around the stoichiometric time linked to the adsorption equilibrium concentration that relates to the feed saturation at equilibrium conditions. Moreover, the quantification of CO₂ loading from the mixture breakthrough curves (shown as empty markers in Figure 1c) reveals that the CO₂ uptake under binary flow conditions closely matches the corresponding single-component values indicating, no competitive adsorption with CH₄. This one-to-one correspondence demonstrates that CH₄ does not effectively compete for adsorption sites, and CO₂ adsorption proceeds as if CH₄ were absent, a hallmark of a kinetically selective adsorption mechanism. Dilution of CO₂ in the feed from 50:50 to 10:90 has only a minor effect on the breakthrough profiles: the CO₂ front remains sharp and CH₄ continues to



elute at the space time of the gas in the bed. Increasing the total pressure from 100 to 500 kPa proportionally enhances CO₂ uptake, consistent with the equilibrium isotherm, while leaving the kinetic exclusion of CH₄ unaffected. This kinetically selective behavior was confirmed by multiple adsorption/desorption cycles performed for a CO₂/CH₄ feed composition of 50:50 vol.%, which yielded highly reproducible breakthrough curves (Figure S15). The CO₂ adsorption capacity remained essentially unchanged over ten consecutive cycles, while CH₄ continued to behave as a non-adsorbing component, indicating the absence of CH₄ accumulation in the material and no loss of separation performance.

To further quantify the kinetic discrimination between CO₂ and CH₄, the breakthrough experiments were modeled using the Aspen Adsorption software, with the simulated profiles shown as continuous lines in Figure 3. In these simulations, the mass-transfer coefficient of CH₄ ($k_{\text{LDF}}(\text{CH}_4)$) at 100 kPa was systematically varied to capture the experimentally observed inert-like behavior of CH₄ with MFU-4. The $k_{\text{LDF}}(\text{CH}_4)$ parameter was progressively reduced until agreement with the experimental breakthrough data was achieved. For $k_{\text{LDF}}(\text{CH}_4) \leq 1.0 \times 10^{-4} \text{ s}^{-1}$, the predicted CH₄ breakthrough curves become insensitive to further decreases in k_{LDF} and fully overlap with the experimental profiles, indicating that this value corresponds to a limiting diffusivity below which CH₄ breakthrough occurs essentially at the gas residence time in the fixed bed. By contrast, the CO₂ breakthrough curve profile is well reproduced with a $k_{\text{LDF}}(\text{CO}_2)$ value of $1.5 \times 10^{-1} \text{ s}^{-1}$, which is approximately three orders of magnitude greater than the one for CH₄. This trend confirms that the transient column response is governed almost exclusively by CO₂ diffusion and adsorption inside the framework, while CH₄ behaves effectively as a dynamically non-adsorbing component, supporting that CO₂/CH₄ separation in MFU-4 is kinetically-governed giving rise to a molecular sieve separation of both components. Aspen Adsorption allows the k_{LDF} to incorporate combined temperature and pressure dependencies, following an Arrhenius-type expression for temperature and a first-order dependency on total pressure (Eq. S7). Within this framework, the k_{LDF} coefficients employed for the breakthrough simulations at 500 kPa were obtained by scaling those determined at 100 kPa by a factor of five. Importantly, using the same $k_{\text{LDF}}(\text{CO}_2)/k_{\text{LDF}}(\text{CH}_4)$ ratio yields excellent agreement with the experimental breakthrough profiles at 500 kPa (Figure 3b and 3d), demonstrating that the pronounced difference in diffusion kinetics between CO₂ and CH₄ is preserved at elevated pressure. This result further confirms that CO₂/CH₄ separation in MFU-4 remains kinetically governed under elevated pressure conditions relevant to industrial operation, with CH₄ continuing to behave as a dynamically non-adsorbing component.

View Article Online
DOI: 10.1039/D6TA01917J



Breakthrough curves at 313 and 343 K, together with their corresponding dynamic simulations, are equally provided in Figures S13 and S14. Although increasing the temperature reduces the overall CO₂ uptake, the qualitative features of the breakthrough profiles remain unchanged: CH₄ elutes at the space time of the gas in the bed whereas CO₂ is selectively adsorbed. The numerical simulations accurately reproduce these experimental profiles, reinforcing the conclusion that MFU-4 maintains strong kinetic sieving behavior over a wide range of operating conditions relevant to natural gas upgrading and biogas purification strategies, especially by PSA. The full set of kinetic parameters for the CO₂ and CH₄ simulations (including k_{∞} , E_i , and k_{LDF} at each temperature and pressure) are provided in Table S8.

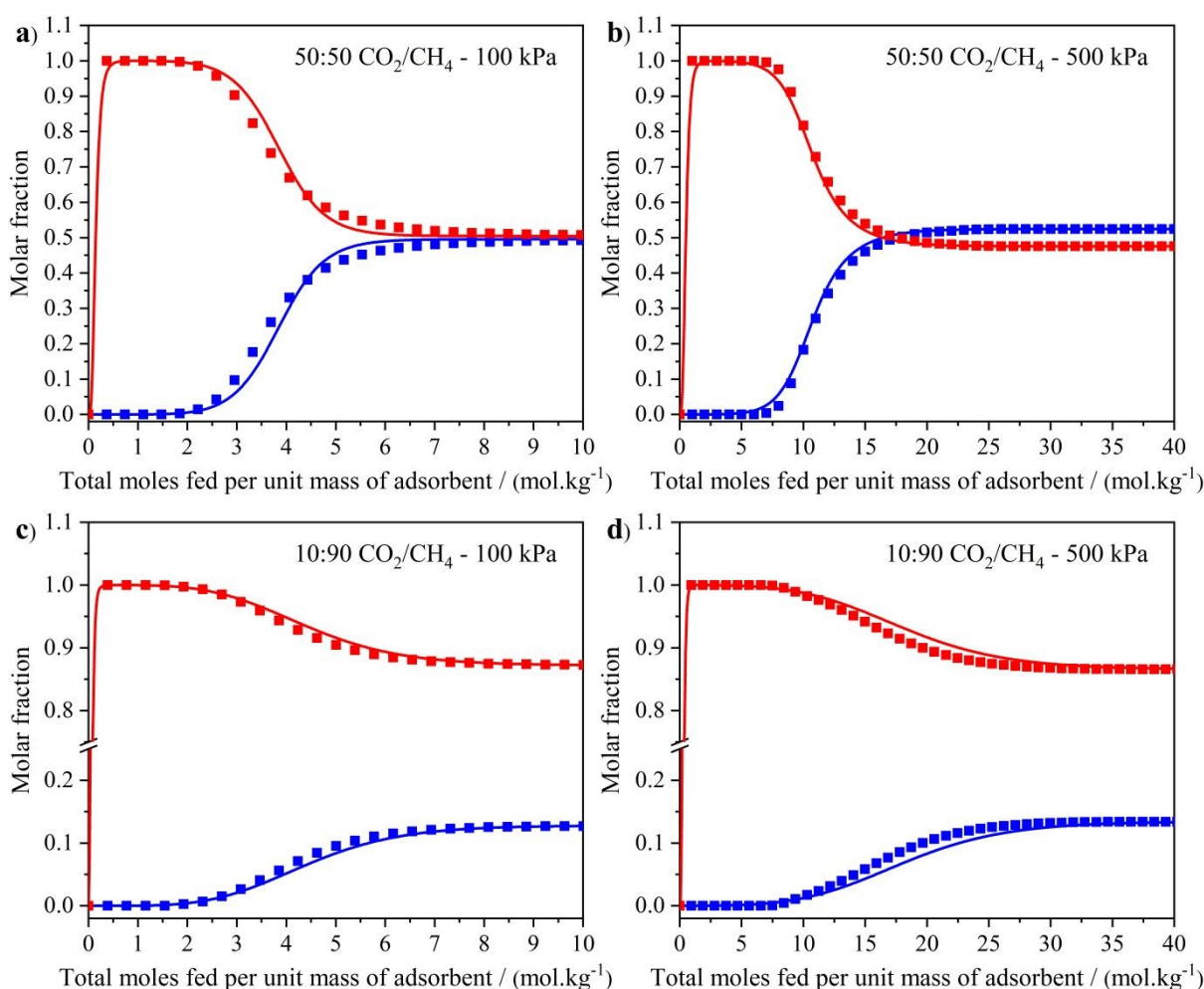


Figure 3. CO₂/CH₄ binary mixtures breakthrough curves on MFU-4 at 298 K. Conditions for each panel are: (a) CO₂/CH₄ 50:50 at 100 kPa, (b) CO₂/CH₄ 50:50 at 500 kPa, (c) CO₂/CH₄ 10:90 at 100 kPa, and (d) CO₂/CH₄ 10:90 at 500 kPa. Data are plotted as component molar fraction (left y-axis) versus total moles fed per unit mass of adsorbent. Symbols represent experimental data, and continuous lines represent numerical simulations.



The performance of MFU-4 was evaluated against the two industrially established benchmark adsorbents CMS-3K and ETS-4, using CO₂ adsorption equilibrium uptake, kinetic selectivity (Habgood formulation, Eq. S10) and working capacity (100-500 kPa, Eq. S11) as key performance metrics. Figure 4a reports the single component CO₂ adsorption isotherms for MFU-4 at near-ambient temperature and the same data reported previously for the benchmark adsorbents ion exchanged ETS-4 and CMS-3K. The comparison highlights that MFU-4 exhibits a much higher CO₂ uptake across the entire pressure range. In particular, MFU-4 reaches a CO₂ loading of ~7.4 mol·kg⁻¹ at 500 kPa, substantially exceeding the uptakes of CMS-3K, Ba-ETS-4 and Sr-ETS-4 which remain below 3.0 mol·kg⁻¹ over the same pressure range. This superior uptake directly translates into outstanding CO₂ working capacities for both (50:50) and (10:90) CO₂/CH₄ mixture feeds over the 100–500 kPa range at 298 K. For a (50:50) mixture, MFU-4 delivers a working capacity of 3.93 mol·kg⁻¹, exceeding those of CMS-3K (0.94 mol·kg⁻¹) and ETS-4 variants (<0.60 mol·kg⁻¹) by more than fourfold and six-fold, respectively (Figures 4b and 4c). Remarkably, even under the more demanding 10:90 feed composition, MFU-4 retains a high working capacity of 1.52 mol·kg⁻¹, outperforming CMS-3K and ETS-4 by approximately two- to fourfold, highlighting its attractiveness under industrially relevant conditions.

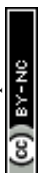
Decisively, this exceptional CO₂ working capacity is coupled with an unprecedented level of kinetic selectivity. MFU-4 attains a kinetic selectivity of 67, outperforming Ba-ETS-4 and Sr-ETS-4 by approximately 90–150% and exceeding CMS-3K by more than 300% (see Table S9 for detailed values). Achieving such simultaneous superiority in both uptake swing and kinetic discrimination is extremely rare in microporous adsorbents and, to date, has not been realized by any industrial benchmarks. In existing technologies based on ETS-4 and CMS-3K, comparable working capacities can only be approached through vacuum-assisted regeneration, which substantially increases the energy penalty and operating costs of VPSA processes.

Beyond this direct comparison with industrial benchmarks, a broader evaluation against representative adsorbents reported for biogas upgrading, primarily governed by thermodynamic separation mechanisms, further highlights the distinctive performance of MFU-4 (see Table S10). In terms of CO₂ adsorption capacity, at 298 K and 100 kPa, MFU-4 exhibits an uptake of 3.61 mol·kg⁻¹, which is higher than that of silica-based materials (~0.3–1.0 mol·kg⁻¹),^[88–90] periodic mesoporous organosilicas (PMOs, ~0.5–1.2 mol·kg⁻¹),^[91] pillared clays (~0.5–1.5 mol·kg⁻¹),^[92] and typical activated carbons (~1.7–2.5 mol·kg⁻¹).^[93–96] With respect to other MOFs, MFU-4 shows a mixed uptake profile: it outperforms several materials, including MIL-101(Cr) (1.49 mol·kg⁻¹),^[97] IITKGP-21a (1.86 mol·kg⁻¹),^[98] CAU-10 (up to 2.3 mol·kg⁻¹),^[99] ZU-301 (2.41 mol·kg⁻¹),^[100] MIL-53 and MIL-125(Ti) (up to 2.64 mol·kg⁻¹),^[9,97,101] UiO-66(Zr)



(up to $2.69 \text{ mol}\cdot\text{kg}^{-1}$),^[101] and others,^[102,103] while remaining comparable to MIL-100 (up to $3.5 \text{ mol}\cdot\text{kg}^{-1}$),^[101] MIL-120(Al) ($3.56 \text{ mol}\cdot\text{kg}^{-1}$),^[43] and MIL-160(Al) ($3.89 \text{ mol}\cdot\text{kg}^{-1}$).^[104] However, lower CO_2 uptake is observed when compared to TAMOF-1,^[105] ZJU-8a,^[106] Cu-BTC,^[101] UTSA-16/120,^[107,108] SIFSIX-type materials,^[108] with values collectively spanning $4.0\text{--}5.5 \text{ mol}\cdot\text{kg}^{-1}$, as well as Mg-MOF-74 ($8.32 \text{ mol}\cdot\text{kg}^{-1}$),^[36] known for its exceptional CO_2 adsorption capacity. A similar trend is observed for zeolites, where MFU-4 exhibits higher uptake than DDR ($1.37 \text{ mol}\cdot\text{kg}^{-1}$),^[109] Na-ZSM-5 ($1.39 \text{ mol}\cdot\text{kg}^{-1}$),^[110] Silicalite-1 ($1.69 \text{ mol}\cdot\text{kg}^{-1}$),^[109] Beta ($2.05 \text{ mol}\cdot\text{kg}^{-1}$),^[109] and 5A ($3.06 \text{ mol}\cdot\text{kg}^{-1}$),^[20] while remaining lower than 4A ($4.29 \text{ mol}\cdot\text{kg}^{-1}$),^[15] 13X ($4.58 \text{ mol}\cdot\text{kg}^{-1}$),^[7] NaX ($4.82 \text{ mol}\cdot\text{kg}^{-1}$),^[101] and NaY ($5.44 \text{ mol}\cdot\text{kg}^{-1}$).^[111] Importantly, at higher pressure (500 kPa), the experimental CO_2 uptake of MFU-4 reaches $\sim 7.36 \text{ mol}\cdot\text{kg}^{-1}$, exceeding the capacity of several materials that outperform it at lower pressure, thereby highlighting its strong adsorption capability across the range relevant for practical applications. Under these conditions, in terms of CO_2 uptake, MFU-4 is only surpassed by a limited number of MOFs, such as ZJU-8a,^[106] Cu-BTC,^[101] and Mg-MOF-74,^[36] with reported values ranging from 10.5 to $12.9 \text{ mol}\cdot\text{kg}^{-1}$.

In terms of adsorption energetics, MFU-4 presents a moderate CO_2 affinity (i.e. Q_{st} of $24.7 \text{ kJ}\cdot\text{mol}^{-1}$), which, relative to high-capacity MOFs, is comparable to that of ZJU-8a ($19.5\text{--}21.9 \text{ kJ}\cdot\text{mol}^{-1}$),^[106] while remaining significantly lower than that of Mg-MOF-74 ($45.3\text{--}72.7 \text{ kJ}\cdot\text{mol}^{-1}$).^[36] This further highlights the favorable balance between adsorption strength and regenerability of MFU-4. In terms of CO_2/CH_4 selectivity, MFU-4 exhibits a high value of 67 when evaluated using the Habgood formulation (Eq. S10), a kinetic-based approach that integrates both equilibrium and kinetic contributions. This value already lies within the upper range of materials collected in Table S10. It is important to note that different approaches are commonly used to evaluate thermodynamic selectivity (see Section S3.2), leading to a wide range of reported values depending on the method employed. To enable a more consistent comparison with materials governed by equilibrium-based separation mechanisms, it is instructive to consider selectivity values derived from breakthrough experiments, which better reflect practical operating conditions. In this context, high selectivities for CO_2/CH_4 mixtures ($\sim 50:50 \text{ vol.}\%$) have been reported for materials such as zeolite 13X (88),^[9] MIL-120 (89.3),^[43] and $\text{NH}_2\text{-MIL-53(Al)}$ (207)^[9] at 100 kPa and 298–303 K. In the case of MFU-4, a fundamentally different behavior is observed. Breakthrough experiments reveal that CH_4 is effectively excluded from the framework due to severe diffusion limitations, resulting in negligible adsorption of this component. Consequently, when selectivity is evaluated directly from dynamic adsorption data, it can be considered essentially infinite for MFU-4.



Taken together, these results demonstrate that MFU-4 represents a step change in adsorbent performance for biogas upgrading, uniquely overcoming the long-standing trade-off between CO₂/CH₄ selectivity and uptake. By combining high working capacity, moderate adsorption energetics, and effectively infinite kinetic selectivity under dynamic conditions, MFU-4 enables high-efficiency separations without reliance on energy-intensive vacuum operation, setting it apart from both industrial benchmarks, such as CMS-3K and ETS-4, and state-of-the-art materials reported in the literature. Beyond separation performance, scalability and synthesis cost are critical considerations for industrial application. In this context, MFU-4 can be synthesized via relatively straightforward solvothermal methods using commercially available precursors, and its components are, in principle, amenable to scale-up. However, there are no detailed studies on the industrial scalability and the production cost of this MOF. As commonly observed in MOF chemistry, the cost associated with ligand and synthesis can be significantly reduced through the development of optimized synthetic routes and bulk production strategies.

View Article Online
DOI: 10.1039/D6TA01917J



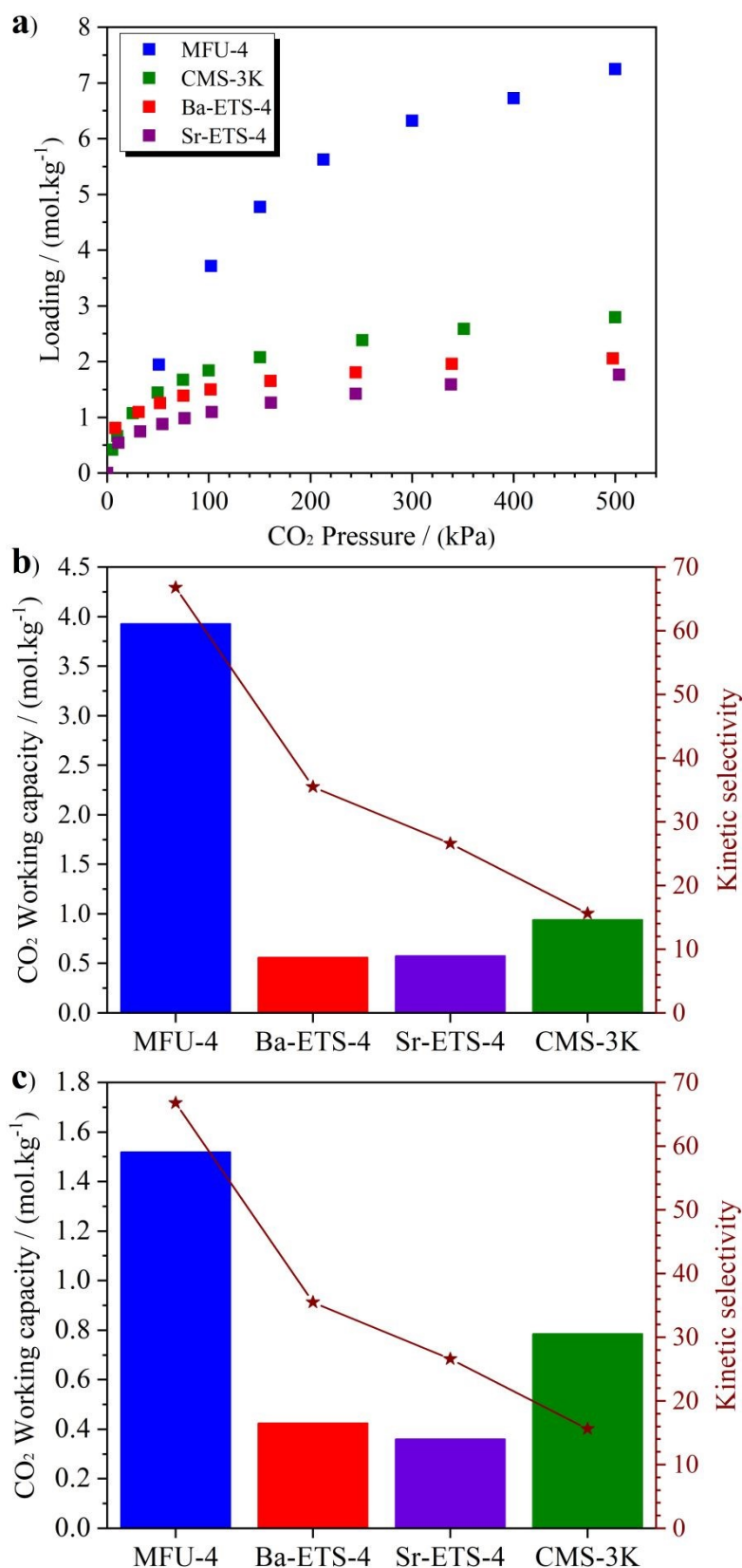


Figure 4. Comparison of MFU-4 performance (this work) with benchmark adsorbents (ETS-4 variants,^[54–56] CMS-3K^[48]) for CO₂/CH₄ separation at near-ambient temperature. **(a)** Equilibrium single-component CO₂ adsorption isotherms at 298 K. **(b-c)** CO₂ working capacity versus kinetic selectivity for **(b)** 50:50 and **(c)** 10:90 CO₂/CH₄ mixtures.



4 Conclusions

View Article Online
DOI: 10.1039/D6TA01917J

In summary, we demonstrate that the ultra-microporous Zn triazolate MOF MFU-4 acts as an exceptionally efficient kinetic molecular sieve for CO₂/CH₄ separation, decisively outperforming industrial benchmark adsorbents such as CMS-3K and ion-exchanged ETS-4. Owing to its favorable architecture, which combines ultra-narrow pore gates with large cavities, MFU-4 uniquely delivers both high kinetic selectivity and high CO₂ working capacity, thereby explicitly breaking the long-standing trade-off between selectivity and uptake that constrains conventional molecular sieves. For a 50:50 CO₂/CH₄ mixture, MFU-4 achieves a CO₂ working capacity of 3.93 mol·kg⁻¹, more than four and six times higher than CMS-3K (0.94 mol·kg⁻¹) and ETS-4 variants (<0.60 mol·kg⁻¹), respectively, while simultaneously reaching an exceptional kinetic selectivity of 67. This unprecedented combination enables efficient cyclic PSA operation over the industrially relevant 100–500 kPa pressure range without the need for vacuum-assisted regeneration. Together, these results establish MFU-4 as a showcase for the development of next-generation MOF adsorbent that redefines performance limits for energy-efficient biogas upgrading. Ongoing efforts should be now directed toward exploring alternative, more scalable synthesis approaches (e.g., reflux-based methods) of MFU-4 to enable larger-scale production while maintaining material performance in order to facilitate its industrial translation.

Acknowledgments

Adriano Henrique and José A. C. Silva acknowledge Portuguese national funds through FCT/MCTES (PIDDAC): CIMO UID/00690/2025 (10.54499/UID/00690/2025) and UID/PRR/00690/2025 (10.54499/UID/PRR/00690/2025); SusTEC, LA/P/0007/2020 (DOI: 10.54499/LA/P/0007/2020). Guillaume Maurin thanks Institut Universitaire de France for the Senior Chair.



References

View Article Online
DOI: 10.1039/D6TA01917J

- [1] I. Angelidaki, L. Treu, P. Tsapekos, G. Luo, S. Campanaro, H. Wenzel, P. G. Kougias, “Biogas upgrading and utilization: Current status and perspectives” *Biotechnol. Adv.* **2018**, *36*, 452–466.
- [2] N. Scarlat, J. F. Dallemand, F. Fahl, “Biogas: developments and perspectives in Europe” *Renew. Energy* **2018**, *129*, 457–472.
- [3] E. Ryckebosch, M. Drouillon, H. Vervaeren, “Techniques for transformation of biogas to biomethane” *Biomass Bioenergy* **2011**, *35*, 1633–1645.
- [4] B. Aghel, S. Behaein, S. Wongwises, M. S. Shadloo, “A review of recent progress in biogas upgrading: with emphasis on carbon capture” *Biomass Bioenergy* **2022**, *160*, 106422.
- [5] A. A. Abd, M. R. Othman, Z. Helwani, J. Kim, “Waste to wheels: performance comparison between pressure swing adsorption and amine-absorption technologies for upgrading biogas containing hydrogen sulfide to fuel grade standards” *Energy* **2023**, *272*, 127060.
- [6] A. Ali Abd, M. Roslee Othman, Z. Helwani, J. Kim, “An overview of biogas upgrading via pressure swing adsorption: Navigating through bibliometric insights towards a conceptual framework and future research pathways” *Energy Convers. Manag.* **2024**, *306*, 118268.
- [7] S. Cavenati, C. A. Grande, A. E. Rodrigues, “Adsorption equilibrium of methane, carbon dioxide, and nitrogen on zeolite 13X at high pressures” *J. Chem. Eng. Data* **2004**, *49*, 1095–1101.
- [8] J. A. C. Silva, K. Schumann, A. E. Rodrigues, “Sorption and kinetics of CO₂ and CH₄ in binderless beads of 13X zeolite” *Microporous and Mesoporous Materials* **2012**, *158*, 219–228.
- [9] S. A. Peter, G. V. Baron, J. Gascon, F. Kapteijn, J. F. M. Denayer, “Dynamic desorption of CO₂ and CH₄ from amino-MIL-53(Al) adsorbent” *Adsorption* **2013**, *19*, 1235–1244.
- [10] J. A. C. Silva, A. F. Cunha, K. Schumann, A. E. Rodrigues, “Binary adsorption of CO₂/CH₄ in binderless beads of 13X zeolite” *Microporous and Mesoporous Materials* **2014**, *187*, 100–107.
- [11] C. A. Grande, R. Blom, “Cryogenic adsorption of methane and carbon dioxide on zeolites 4A and 13X” *Energy and Fuels* **2014**, *28*, 6688–6693.
- [12] F. A. Abdul Kareem, A. M. Shariff, S. Ullah, N. Mellon, L. K. Keong, “Adsorption of pure and predicted binary (CO₂:CH₄) mixtures on 13X-zeolite: equilibrium and kinetic properties at offshore conditions” *Microporous and Mesoporous Materials* **2018**, *267*, 221–234.
- [13] A. Streb, M. Mazzotti, “Adsorption for efficient low carbon hydrogen production: part 1-adsorption equilibrium and breakthrough studies for H₂/CO₂/CH₄ on zeolite 13X” *Adsorption* **2021**, *27*, 541–558.



- [14] H. Jedli, S. M. Bouzgarrou, R. Hassani, E. Sabi, K. Slimi, “Adsorption of CO₂, CH₄ and H₂ onto zeolite 13 X: Kinetic and equilibrium studies” *Heliyon* **2024**, *10*, e40672. DOI: 10.1039/D6TA01917J
- [15] K. G. Wynnyk, B. Hojjati, P. Pirzadeh, R. A. Marriott, “High-pressure sour gas adsorption on zeolite 4A” *Adsorption* **2017**, *23*, 149–162.
- [16] R. Seabra, A. M. Ribeiro, K. Gleichmann, A. F. P. Ferreira, A. E. Rodrigues, “Adsorption equilibrium and kinetics of carbon dioxide, methane and nitrogen on binderless zeolite 4A adsorbents” *Microporous and Mesoporous Materials* **2019**, *277*, 105–114.
- [17] L. F. A. S. Zafanelli, A. Henrique, M. Karimi, A. E. Rodrigues, J. A. C. Silva, “Single- and multicomponent fixed bed adsorption of CO₂, CH₄, and N₂ in binder-free beads of 4A zeolite” *Ind. Eng. Chem. Res.* **2020**, *59*, 13724–13734.
- [18] S. Duan, Y. Xie, H. Yin, P. Shen, “Investigation of CO₂, CH₄ and N₂ adsorption mechanism on zeolite 4A using statistical physics and site energy distribution analysis” *Microporous and Mesoporous Materials* **2025**, *398*.
- [19] D. Saha, Z. Bao, F. Jia, S. Deng, “Adsorption of CO₂, CH₄, N₂O, and N₂ on MOF-5, MOF-177, and zeolite 5A” *Environ. Sci. Technol.* **2010**, *44*, 1820–1826.
- [20] M. Mofarahi, F. Gholipour, “Gas adsorption separation of CO₂/CH₄ system using zeolite 5A” *Microporous and Mesoporous Materials* **2014**, *200*, 1–10.
- [21] M. I. Hossain, B. D. Rabideau, T. G. Glover, “The impact of trace amounts of CO₂ on the high-pressure adsorption of CH₄ on 5A zeolite” *Microporous and Mesoporous Materials* **2024**, *369*, DOI 10.1016/j.micromeso.2023.112948.
- [22] S. R. Jeong, K. M. Kim, C. H. Lee, “Adsorption equilibria and kinetics of CO₂, CO, CH₄, N₂, and H₂ on zeolite 5 A up to 1.0 MPa” *Chemical Engineering Journal* **2025**, *525*.
- [23] X. Xu, X. Zhao, L. Sun, X. Liu, “Adsorption separation of carbon dioxide, methane, and nitrogen on Hβ and Na-exchanged β-zeolite” *Journal of Natural Gas Chemistry* **2008**, *17*, 391–396.
- [24] J. Yang, Q. Zhao, H. Xu, L. Li, J. Dong, J. Li, “Adsorption of CO₂, CH₄, and N₂ on gas diameter grade ion-exchange small pore zeolites” *J. Chem. Eng. Data* **2012**, *57*, 3701–3709.
- [25] Y. Li, H. Yi, X. Tang, F. Li, Q. Yuan, “Adsorption separation of CO₂/CH₄ gas mixture on the commercial zeolites at atmospheric pressure” *Chemical Engineering Journal* **2013**, *229*, 50–56.
- [26] P. A. S. Moura, D. P. Bezerra, E. Vilarrasa-Garcia, M. Bastos-Neto, D. C. S. Azevedo, “Adsorption equilibria of CO₂ and CH₄ in cation-exchanged zeolites 13X” *Adsorption* **2016**, *22*, 71–80.
- [27] H. Golipour, B. Mokhtarani, M. Mafi, M. Khadivi, H. R. Godini, “Systematic measurements of CH₄ and CO₂ adsorption isotherms on cation-exchanged zeolites 13X” *J. Chem. Eng. Data* **2019**, *64*, 4412–4423.



- [28] H. Golipour, B. Mokhtarani, M. Mafi, M. Khadivi, H. R. Godini, “Systematic Measurements of CH₄ and CO₂ Adsorption Isotherms on Cation-Exchanged Zeolites 13X” *J. Chem. Eng. Data* **2019**, *64*, 4412–4423. Article Online
DOI: 10.1039/D6TA01917J
- [29] L. Feng, Y. Shen, T. Wu, B. Liu, D. Zhang, Z. Tang, “Adsorption equilibrium isotherms and thermodynamic analysis of CH₄, CO₂, CO, N₂ and H₂ on NaY Zeolite” *Adsorption* **2020**, *26*, 1101–1111.
- [30] E. Aly, L. F. A. S. Zafanelli, A. Henrique, M. Golini Pires, A. E. Rodrigues, K. Gleichmann, J. A. C. Silva, “Fixed bed adsorption of CO₂, CH₄, and N₂ and their mixtures in potassium-exchanged binder-free beads of Y zeolite” *Ind. Eng. Chem. Res.* **2021**, *60*, 15236–15247.
- [31] A. M. Najafi, F. Khorasheh, S. Soltanali, H. Ghassabzadeh, “Equilibrium and kinetic insights into the comprehensive investigation of CO₂, CH₄, and N₂ adsorption on cation-exchanged X and Y faujasite zeolites” *Langmuir* **2023**, *39*, 15535–15546.
- [32] Y. Sun, H. Li, H. Lai, Y. Yu, M. Hou, C. Fu, Z. Wang, C. Zhang, “CO₂ selective adsorption from CO₂/CH₄ mixtures and regeneration of X zeolites by Li and K modification using various regeneration strategies” *Chemical Engineering Journal* **2025**, *515*, 163682.
- [33] B. Achenbach, A. Yurdusen, N. Stock, G. Maurin, C. Serre, “Synthetic aspects and characterization needs in MOF chemistry – from discovery to applications” *Advanced Materials* **2025**, 2411359.
- [34] S. R. Caskey, A. G. Wong-Foy, A. J. Matzger, “Dramatic tuning of carbon dioxide uptake via metal substitution in a coordination polymer with cylindrical pores” *J. Am. Chem. Soc.* **2008**, *130*, 10870–10871.
- [35] J. A. Mason, K. Sumida, Z. R. Herm, R. Krishna, J. R. Long, “Evaluating metal-organic frameworks for post-combustion carbon dioxide capture via temperature swing adsorption” *Energy Environ. Sci.* **2011**, *4*, 3030–3040.
- [36] Z. Bao, L. Yu, Q. Ren, X. Lu, S. Deng, “Adsorption of CO₂ and CH₄ on a magnesium-based metal organic framework” *J. Colloid Interface Sci.* **2011**, *353*, 549–556.
- [37] T. M. McDonald, W. R. Lee, J. A. Mason, B. M. Wiers, C. S. Hong, J. R. Long, “Capture of carbon dioxide from air and flue gas in the alkylamine-appended metal-organic framework mmen-Mg₂(dobpdc)” *J. Am. Chem. Soc.* **2012**, *134*, 7056–7065.
- [38] T. M. McDonald, J. A. Mason, X. Kong, E. D. Bloch, D. Gygi, A. Dani, V. Crocellà, F. Giordanino, S. O. Odoh, W. S. Drisdell, B. Vlasisavljevich, A. L. Dzubak, R. Poloni, S. K. Schnell, N. Planas, K. Lee, T. Pascal, L. F. Wan, D. Prendergast, J. B. Neaton, B. Smit, J. B. Kortright, L. Gagliardi, S. Bordiga, J. A. Reimer, J. R. Long, “Cooperative insertion of CO₂ in diamine-appended metal-organic frameworks” *Nature* **2015**, *519*, 303–308.
- [39] W. R. Lee, H. Jo, L. M. Yang, H. Lee, D. W. Ryu, K. S. Lim, J. H. Song, D. Y. Min, S. S. Han, J. G. Seo, Y. K. Park, D. Moon, C. S. Hong, “Exceptional CO₂ working capacity in a heterodiamine-grafted metal-organic framework” *Chem. Sci.* **2015**, *6*, 3697–3705.
- [40] E. J. Kim, R. L. Siegelman, H. Z. H. Jiang, A. C. Forse, J. H. Lee, J. D. Martell, P. J. Milner, J. M. Falkowski, J. B. Neaton, J. A. Reimer, S. C. Weston, J. R. Long,



“Cooperative carbon capture and steam regeneration with tetraamine-appended metal-organic frameworks” *Science* **2020**, *369*, 392–396. Article Online
DOI: 10.1039/D6TA01917J

- [41] R. P. Loughran, T. Hurley, A. Gładysiak, A. Chidambaram, K. Khivantsev, E. D. Walter, T. R. Graham, P. Reardon, J. Szanyi, D. B. Fast, Q. R. S. Miller, A. H. A. Park, K. C. Stylianou, “CO₂ capture from wet flue gas using a water-stable and cost-effective metal-organic framework” *Cell Rep. Phys. Sci.* **2023**, *4*, 101470.
- [42] B. Chen, D. Fan, R. V. Pinto, I. Dovgaliuk, S. Nandi, D. Chakraborty, N. García-Moncada, A. Vimont, C. J. McMonagle, M. Bordonhos, A. Al Mohtar, I. Cornu, P. Florian, N. Heymans, M. Daturi, G. De Weireld, M. Pinto, F. Nouar, G. Maurin, G. Mouchaham, C. Serre, “A scalable robust microporous Al-MOF for post-combustion carbon capture” *Advanced Science* **2024**, *11*, 2401070.
- [43] M. Bordonhos, R. V. Pinto, T. Frade, B. Chen, F. Nouar, G. Mouchaham, J. R. B. Gomes, C. Serre, M. L. Pinto, “Towards sustainable biogas upgrading: MIL-120(Al) as a cost-effective water stable MOF for CO₂/CH₄ separation” *J. Mater. Chem. A Mater.* **2026**, *14*, 12856–12866.
- [44] J.-B. Lin, T. T. T. Nguyen, R. Vaidhyathan, J. Burner, J. M. Taylor, H. Durekova, F. Akhtar, R. K. Mah, O. Ghaffari-Nik, S. Marx, N. Fylstra, S. S. Iremonger, K. W. Dawson, P. Sarkar, P. Hovington, A. Rajendran, T. K. Woo, G. K. H. Shimizu, “A scalable metal-organic framework as a durable physisorbent for carbon dioxide capture” *Science* **2021**, *374*, 1464–1469.
- [45] P. M. Bhatt, Y. Belmabkhout, A. Cadiou, K. Adil, O. Shekhah, A. Shkurenko, L. J. Barbour, M. Eddaoudi, “A fine-tuned fluorinated MOF addresses the needs for trace CO₂ removal and air capture using physisorption” *J. Am. Chem. Soc.* **2016**, *138*, 9301–9307.
- [46] D. M. Ruthven, *Principles of Adsorption and Adsorption Processes*, John Wiley & Sons, **1984**.
- [47] R. T. Yang, *Adsorbents: Fundamentals and Applications*, John Wiley & Sons, **2003**.
- [48] S. Cavenati, *Separação de Misturas CH₄/CO₂/N₂ Por Processos Adsorptivos*, Faculdade de Engenharia da Universidade do Porto, **2005**.
- [49] S. Cavenati, C. A. Grande, A. E. Rodrigues, “Upgrade of methane from landfill gas by pressure swing adsorption” *Energy and Fuels* **2005**, *19*, 2545–2555.
- [50] SysAdvance, *Energy - Biogas Upgrading | H₂S Reduction (Technical Brochure)*, **2023**.
- [51] SysAdvance, *Industrial - Nitrogen Series | Oxygen Series | Helisys | OxygenVSA (Technical Brochure)*, **2023**.
- [52] S. M. Kuznicki, *Preparation of Small-Pored Crystalline Titanium Molecular Sieve Zeolites*, **1990**, *4*, 938,939.
- [53] S. M. Kuznicki, V. A. Bell, S. Nair, H. W. Hillhouse, R. M. Jacobinas, C. M. Braunbarth, B. H. Toby, M. Tsapatsis, “A titanosilicate molecular sieve with adjustable pores for size-selective adsorption of molecules” *Nature* **2001**, *412*, 720–724.



- [54] R. P. Marathe, S. Farooq, M. P. Srinivasan, “Modeling gas adsorption and transport in small-pore titanium silicates” *Langmuir* **2005**, *21*, 4532–4546. Article Online
DOI: 10.1039/D6TA01917J
- [55] B. Majumdar, S. J. Bhadra, R. P. Marathe, S. Farooq, “Adsorption and diffusion of methane and nitrogen in barium exchanged ETS-4” *Ind. Eng. Chem. Res.* **2011**, *50*, 3021–3034.
- [56] Q. Peng, Y. Chen, D. Fang, C. Liu, K. Wu, Y. Chen, H. Jiang, Y. Sun, Q. Wu, D. Wu, H. Sun, “Enhancing size-selective adsorption of CO₂/CH₄ on ETS-4 via ion-exchange coupled with thermal treatment” *Ind. Eng. Chem. Res.* **2023**, *62*, 9313–9324.
- [57] Guild Associates, “Molecular Gate® Adsorbent Technology,” can be found under <https://www.guildassociates.com/gas-processing-systems/mgtech/>
- [58] M. Azadi Tabar, E. Pancione, S. A. Peter, J. F. M. Denayer, “Four-column vacuum pressure swing adsorption for biogas upgrading with co-production of high-purity biogenic CO₂: experimental and simulation study” *Journal of CO₂ Utilization* **2026**, *105*, 103348.
- [59] S. Biswas, M. Grzywa, H. P. Nayek, S. Dehnen, I. Senkowska, S. Kaskel, D. Volkmer, “A cubic coordination framework constructed from benzobistriazolate ligands and zinc ions having selective gas sorption properties” *Dalton Transactions* **2009**, 6487–6495.
- [60] H. Hart, D. Ok, “Synthesis of 1,5-diamino-1,5-dihydrobenzo[1,2-d:4,5-d']bistriazole (DABT) and its use as a 1,4-benzadiyne equivalent” *J. Org. Chem.* **1986**, *51*, 979–986.
- [61] Aspentech, *Aspen Adsim™ 11.1 - Adsorption Reference Guide*, Cambridge, **2001**.
- [62] D. D. Do, *Adsorption Analysis: Equilibria and Kinetics*, Imperial College Press, **1998**.
- [63] S. Sircar, J. R. Hufton, “Why does the linear driving force model for adsorption kinetics work?” *Adsorption* **2000**, *6*, 137–147.
- [64] A. Henrique, A. E. Rodrigues, J. A. C. Silva, “Separation of hexane isomers in ZIF-8 by fixed bed adsorption” *Ind. Eng. Chem. Res.* **2019**, *58*, 378–394.
- [65] A. Henrique, A. E. Rodrigues, J. A. C. Silva, “Fixed bed dynamics of single and multicomponent adsorption of pentane and hexane isomers in ZIF-8” *Sep. Purif. Technol.* **2020**, *238*, 116419.
- [66] G. Kresse, J. Furthmüller, “Efficient iterative schemes for ab initio total-energy calculations using a plane-wave basis set” *Phys. Rev. B* **1996**, *54*, 11169–11186.
- [67] J. P. Perdew, K. Burke, M. Ernzerhof, “Generalized gradient approximation made simple” *Phys. Rev. Lett.* **1996**, *77*, 3865–3868.
- [68] P. E. Blochl, “Projector augmented-wave method” *Phys. Rev. B* **1994**, *50*, 17953–17979.
- [69] S. Grimme, “Semiempirical GGA-type density functional constructed with a long-range dispersion correction” *J. Comput. Chem.* **2006**, *27*, 1787–1799.
- [70] S. Grimme, S. Ehrlich, L. Goerigk, “Effect of the damping function in dispersion corrected density functional theory” *J. Comput. Chem.* **2011**, *32*, 1456–1465.



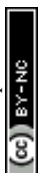
- [71] H. J. Monkhorst, J. D. Pack, “Special points for Brillouin-zone integrations” *Phys. Rev. B* **1976**, *13*, 5188–5192. Article Online
DOI: 10.1039/D6TA01917J
- [72] T. A. Manz, N. G. Limas, “Introducing DDEC6 atomic population analysis: Part 1. Charge partitioning theory and methodology” *RSC Adv.* **2016**, *6*, 47771–47801.
- [73] N. G. Limas, T. A. Manz, “Introducing DDEC6 atomic population analysis: Part 2. Computed results for a wide range of periodic and nonperiodic materials” *RSC Adv.* **2016**, *6*, 45727–45747.
- [74] T. A. Manz, “Introducing DDEC6 atomic population analysis: Part 3. Comprehensive method to compute bond orders” *RSC Adv.* **2017**, *7*, 45552–45581.
- [75] N. G. Limas, T. A. Manz, “Introducing DDEC6 atomic population analysis: Part 4. Efficient parallel computation of net atomic charges, atomic spin moments, bond orders, and more” *RSC Adv.* **2018**, *8*, 2678–2707.
- [76] J. G. Harris, K. H. Yungt, “Carbon dioxide’s liquid-vapor coexistence curve and critical properties as predicted by a simple molecular model” *J. Phys. Chem.* **1995**, *99*, 12021–12024.
- [77] M. G. Martin, J. I. Siepmann, “Transferable potentials for phase equilibria. 1. United-atom description of n-alkanes” *J. Phys. Chem. B* **1998**, *102*, 2569–2577.
- [78] A. K. Rappé, C. J. Casewit, K. S. Colwell, W. A. Goddard, W. M. Skiff, “UFF, a full periodic table force field for molecular mechanisms and molecular dynamics simulations” *J. Am. Chem. Soc.* **1992**, *114*, 10024–10035.
- [79] Q. Yang, C. Zhong, “Molecular simulation of carbon dioxide/methane/hydrogen mixture adsorption in metal-organic frameworks” *J. Phys. Chem. B* **2006**, *110*, 17776–17783.
- [80] T. J. H. Vlugt, E. García-Pérez, D. Dubbeldam, S. Ban, S. Calero, “Computing the heat of adsorption using molecular simulations: The effect of strong Coulombic interactions” *J. Chem. Theory Comput.* **2008**, *4*, 1107–1118.
- [81] G. Henkelman, B. P. Uberuaga, H. Jónsson, “A climbing image nudged elastic band method for finding saddle points and minimum energy paths” *J. Chem. Phys.* **2000**, *113*, 9901–9904.
- [82] T. D. Kühne, M. Iannuzzi, M. Del Ben, V. V. Rybkin, P. Seewald, F. Stein, T. Laino, R. Z. Khaliullin, O. Schütt, F. Schiffmann, D. Golze, J. Wilhelm, S. Chulkov, M. H. Bani-Hashemian, V. Weber, U. Borštnik, M. Taillefumier, A. S. Jakobovits, A. Lazzaro, H. Pabst, T. Müller, R. Schade, M. Guidon, S. Andermatt, N. Holmberg, G. K. Schenter, A. Hehn, A. Bussy, F. Belleflamme, G. Tabacchi, A. Glöß, M. Lass, I. Bethune, C. J. Mundy, C. Plessl, M. Watkins, J. VandeVondele, M. Krack, J. Hutter, “CP2K: An electronic structure and molecular dynamics software package - Quickstep: Efficient and accurate electronic structure calculations” *J. Chem. Phys.* **2020**, *152*, 194103.
- [83] J. VandeVondele, J. Hutter, “Gaussian basis sets for accurate calculations on molecular systems in gas and condensed phases” *J. Chem. Phys.* **2007**, *127*, 144105.
- [84] S. Goedecker, M. Teter, J. Hutter, “Separable dual-space Gaussian pseudopotentials” *Phys. Rev. B* **1996**, *54*, 1703–1710.



- [85] M. Krack, “Pseudopotentials for H to Kr optimized for gradient-corrected exchange-correlation functionals” *Theor. Chem. Acc.* **2005**, *114*, 145–152. Article Online
DOI: 10.1039/D6TA01917J
- [86] M. Thommes, K. Kaneko, A. V. Neimark, J. P. Olivier, F. Rodriguez-Reinoso, J. Rouquerol, K. S. W. Sing, “Physisorption of gases, with special reference to the evaluation of surface area and pore size distribution (IUPAC technical report)” *Pure and Applied Chemistry* **2015**, *87*, 1051–1069.
- [87] G. Sastre, J. Van Den Bergh, F. Kapteijn, D. Denysenko, D. Volkmer, “Unveiling the mechanism of selective gate-driven diffusion of CO₂ over N₂ in MFU-4 metal-organic framework” *Dalton Transactions* **2014**, *43*, 9612–9619.
- [88] Y. Belmabkhout, A. Sayari, “Adsorption of CO₂ from dry gases on MCM-41 silica at ambient temperature and high pressure. 2: Adsorption of CO₂/N₂, CO₂/CH₄ and CO₂/H₂ binary mixtures” *Chem. Eng. Sci.* **2009**, *64*, 3729–3735.
- [89] L. Mafra, T. Čendak, S. Schneider, P. V. Wiper, J. Pires, J. R. B. Gomes, M. L. Pinto, “Amine functionalized porous silica for CO₂/CH₄ separation by adsorption: Which amine and why” *Chemical Engineering Journal* **2018**, *336*, 612–621.
- [90] M. Pacheco, M. Bordonhos, M. Sardo, R. Afonso, J. R. B. Gomes, L. Mafra, M. L. Pinto, “Moisture effect on the separation of CO₂/CH₄ mixtures with amine-functionalised porous silicas” *Chemical Engineering Journal* **2022**, *443*, 136271.
- [91] M. A. O. Lourenço, C. Siquet, M. Sardo, L. Mafra, J. Pires, M. Jorge, M. L. Pinto, P. Ferreira, J. R. B. Gomes, “Interaction of CO₂ and CH₄ with functionalized periodic mesoporous phenylene-silica: periodic DFT calculations and gas adsorption measurements” *Journal of Physical Chemistry C* **2016**, *120*, 3863–3875.
- [92] J. Pires, V. K. Saini, M. L. Pinto, “Studies on selective adsorption of biogas components on pillared clays: Approach for biogas improvement” *Environ. Sci. Technol.* **2008**, *42*, 8727–8732.
- [93] C. A. Grande, R. Blom, A. Möller, J. Möllmer, “High-pressure separation of CH₄/CO₂ using activated carbon” *Chem. Eng. Sci.* **2013**, *89*, 10–20.
- [94] N. Álvarez-Gutiérrez, M. V. Gil, F. Rubiera, C. Pevida, “Adsorption performance indicators for the CO₂/CH₄ separation: Application to biomass-based activated carbons” *Fuel Processing Technology* **2016**, *142*, 361–369.
- [95] N. Álvarez-Gutiérrez, S. García, M. V. Gil, F. Rubiera, C. Pevida, “Dynamic performance of biomass-based carbons for CO₂/CH₄ separation. Approximation to a pressure swing adsorption process for biogas upgrading” *Energy and Fuels* **2016**, *30*, 5005–5015.
- [96] I. Durán, N. Álvarez-Gutiérrez, F. Rubiera, C. Pevida, “Biogas purification by means of adsorption on pine sawdust-based activated carbon: Impact of water vapor” *Chemical Engineering Journal* **2018**, *353*, 197–207.
- [97] N. Singh, S. Dalakoti, A. Sharma, R. Chauhan, R. S. Murali, S. Divekar, S. Dasgupta, Aarti, “Shaping of MIL-53-Al and MIL-101 MOF for CO₂/CH₄, CO₂/N₂ and CH₄/N₂ separation” *Sep. Purif. Technol.* **2024**, *341*.



- [98] R. Sahoo, B. Pramanik, R. Krishna, M. C. Das, “A chemically robust 3D interpenetrated MOF toward one-step methane purification along with six other multipurpose gas separations” *Small* **2026**, *22*, e72629. Article Online
DOI: 10.1039/D6TA01917J
- [99] A. D. Wiersum, C. Giovannangeli, D. Vincent, E. Bloch, H. Reinsch, N. Stock, J. S. Lee, J. S. Chang, P. L. Llewellyn, “Experimental screening of porous materials for high pressure gas adsorption and evaluation in gas separations: application to MOFs (MIL-100 and CAU-10)” *ACS Comb. Sci.* **2013**, *15*, 111–119.
- [100] C. Yu, Q. Ding, J. Hu, Q. Wang, X. Cui, H. Xing, “Selective capture of carbon dioxide from humid gases over a wide temperature range using a robust metal–organic framework” *Chemical Engineering Journal* **2021**, *405*, 126937.
- [101] A. D. Wiersum, J. S. Chang, C. Serre, P. L. Llewellyn, “An adsorbent performance indicator as a first step evaluation of novel sorbents for gas separations: application to metal-organic frameworks” *Langmuir* **2013**, *29*, 3301–3309.
- [102] D. Lv, R. Shi, Y. Chen, Y. Chen, H. Wu, X. Zhou, H. Xi, Z. Li, Q. Xia, “Selective adsorptive separation of CO₂/CH₄ and CO₂/N₂ by a water resistant zirconium-porphyrin metal-organic framework” *Ind. Eng. Chem. Res.* **2018**, *57*, 12215–12224.
- [103] H. N. Wamba, S. Dalakoti, N. Singh, S. Divekar, J. Ngoune, A. Arya, S. Dasgupta, “Facile aqueous medium synthesis of highly stable Zr-MOFs with promising CO₂/CH₄ adsorption selectivity for natural gas and biogas upgradation” *Ind. Eng. Chem. Res.* **2023**, *62*, 19773–19783.
- [104] M. Bordonhos, M. I. S. Neves, A. Marandi, F. Nouar, M. Jorge, J. R. B. Gomes, C. Serre, M. L. Pinto, “Spanning the molecular to industrial scale of the adsorption-based separation of CO₂/CH₄ by MIL-160(Al)” *Chemical Engineering Journal* **2025**, *524*, 169276.
- [105] S. Capelo-Avilés, M. de Fez-Febré, S. R. G. Balestra, J. Cabezas-Giménez, R. Tomazini de Oliveira, I. I. Gallo Stampino, A. Vidal-Ferran, J. González-Cobos, V. Lillo, O. Fabelo, E. C. Escudero-Adán, L. R. Falvello, J. B. Parra, P. Rumori, G. Turnes Palomino, C. Palomino Cabello, S. Giancola, S. Calero, J. R. Galán-Mascarós, “Selective adsorption of CO₂ in TAMOF-1 for the separation of CO₂/CH₄ gas mixtures” *Nature Communications* **2025**, *16*, 3243.
- [106] J. Cai, H. Wang, H. Wang, X. Duan, Z. Wang, Y. Cui, Y. Yang, B. Chen, G. Qian, “An amino-decorated NbO-type metal-organic framework for high C₂H₂ storage and selective CO₂ capture” *RSC Adv.* **2015**, *5*, 77417–77422.
- [107] S. Xiang, Y. He, Z. Zhang, H. Wu, W. Zhou, R. Krishna, B. Chen, “Microporous metal-organic framework with potential for carbon dioxide capture at ambient conditions” *Nat. Commun.* **2012**, *3*.
- [108] H. M. Wen, C. Liao, L. Li, A. Alsalmé, Z. Allothman, R. Krishna, H. Wu, W. Zhou, J. Hu, B. Chen, “A metal-organic framework with suitable pore size and dual functionalities for highly efficient post-combustion CO₂ capture” *J. Mater. Chem. A Mater.* **2019**, *7*, 3128–3134.



- [109] J. Yang, J. Li, W. Wang, L. Li, J. Li, “Adsorption of CO₂, CH₄, and N₂ on 8-, 10-, and 12-membered ring hydrophobic microporous high-silica zeolites: DDR, Silicalite-1, and Beta” *Ind. Eng. Chem. Res.* **2013**, *52*, 17856–17864. View Article Online
DOI: 10.1039/D6TA01917J
- [110] M. Rahmani, B. Mokhtarani, M. Mafi, N. Rahmanian, “Acid gas removal by superhigh silica ZSM-5: adsorption isotherms of hydrogen sulfide, carbon dioxide, methane, and nitrogen” *Ind. Eng. Chem. Res.* **2022**, *61*, 6600–6610.
- [111] A. Sharma, A. Verma, U. Kumar, N. Singh, S. Dalakoti, R. Chauhan, S. Bhandari, S. Divekar, S. Dasgupta, Aarti, “Interchangeable effect of polyols-based zeolite on the separation of CO₂, CH₄, and N₂ gases” *Microporous and Mesoporous Materials* **2024**, *367*, 112984.



Data Availability Statement

View Article Online
DOI: 10.1039/D6TA01917J

The experimental adsorption isotherms, breakthrough data, characterization results, and modeling parameters are provided in the Electronic Supplementary Information (ESI). Additional raw data, including detailed breakthrough profiles and molecular simulation inputs and outputs, are available from the corresponding authors upon reasonable request.

